

pubs.acs.org/acsapm Article

# Engineering Ionomer—Substrate Interface to Improve Thin-Film Proton Conductivity in Proton Exchange Membrane Fuel Cells

Oghenetega Allen Obewhere and Shudipto Konika Dishari\*



Cite This: ACS Appl. Polym. Mater. 2024, 6, 4535-4546



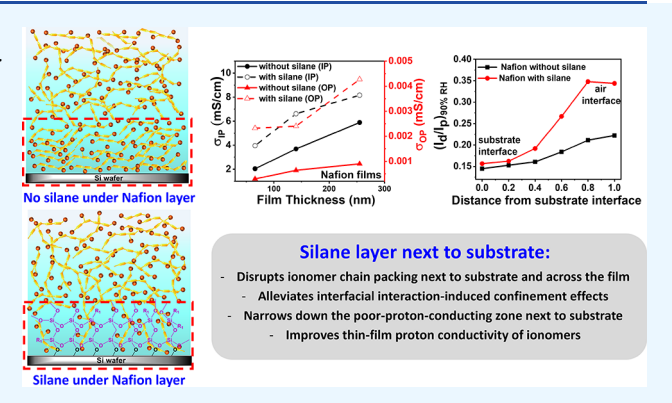
**ACCESS** 

III Metrics & More

Article Recommendations

SI Supporting Information

**ABSTRACT:** Interfacial confinement-induced weak proton conduction in sub- $\mu$ m-thick ionomer films impacts the performance of electrochemical devices. In such films, a fraction of ionomer chains align parallel next to the substrates. The ionomer–substrate interaction pins the chains to the substrate, limiting proton conductivity across the film. We addressed this interfacial chainpinning and ion transport limitation by covalently immobilizing (3-aminopropyl)triethoxysilane (APTES) on  $SiO_2$  before depositing Nafion films ( $\sim$ 60–700 nm thick) on top of it. The silane layer reduced the ionomer chain density next to the substrate (scanning electron microscopy with energy dispersive X-ray spectroscopy) and disrupted the chain packing and orientation within Nafion films (grazing incidence small-angle X-ray scattering, ellipsometry). These changes, especially the suppression of surface-parallel lamella,



effectively minimized the substrate-pinning of Nafion chains, reduced film stiffness, narrowed down the poorly proton-conducting region next to the substrate (confocal laser scanning microscopy), and improved both in-plane (~2 times) and out-of-plane (about an order of magnitude) proton conductivity of Nafion thin films (electrochemical impedance spectroscopy). This work pointed toward a simple but effective surface engineering approach to improve thin-film proton conductivity as well as inform and guide the design of better ionomer—catalyst interfaces for H-fuel cells and other electrochemical devices.

KEYWORDS: Nafion, ionomer, thin film, proton conductivity, interface, fuel cell, catalyst, energy, electrochemical device, surface engineering

# ■ INTRODUCTION

Electrochemical energy conversion and storage devices are springing forth as ecofriendly means to electrify automobiles and appliances. The proton exchange membrane fuel cell (PEMFC) is one such attractive technology that does not emit harmful greenhouse gases while producing electricity using H<sub>2</sub>. While PEMFC holds great promise, its power performance is impacted by the sluggish oxygen reduction reaction (ORR) at the cathode of the cell. To improve the ORR kinetics, we must overcome O2 and proton transport limitations at the catalyst interfaces of PEMFC cathodes.<sup>1-5</sup> The current benchmark ionomer, Nafion conducts protons poorly in sub um thick films, 6-12 interfacing catalyst particles on cathode where ORR occurs. Thus, understanding and appropriately engineering the interface between the catalyst and sub-µm-thick ionomer layers on electrodes are critical to overcoming proton transport limitation.

In sub- $\mu$ m-thick films, ionomer chains experience geometric confinement<sup>7,13</sup> which is not evident in several tens of  $\mu$ m-thick bulk membrane separators made with the same ionomers.<sup>7,9</sup> The confinement effect is exaggerated by interfacial interaction-induced entrapment and interfacial

processes<sup>13</sup> which critically control ionomer behavior across thin films. For example, in ionomer films deposited on SiO<sub>2</sub><sup>7,14</sup> or Pt, <sup>15–19</sup> Nafion chains interact with the substrate and water molecules residing next to the substrate interface. Neutron reflectometry<sup>18,20–22</sup> revealed that, in hydrated films, ionomer chains form several nm-thick lamellar layers next to substrates (SiO<sub>2</sub>, Pt, C) which are often water-rich, and the rest of the film is more bulk-like with random ionomer—water distribution. In this next-to-substrate region, ionomer chains preferentially orient their backbones parallel to the substrate, while their side chains (–SO<sub>3</sub>H-terminated) face the substrate. <sup>4,23–27</sup> This orientation favors interfacial interactions among silanol (–SiOH) groups of substrate, water, and –SO<sub>3</sub>H groups of Nafion chains lying flat on the surface. As a result, ionomer chains and water get pinned to the

Received: January 2, 2024 Revised: March 11, 2024 Accepted: March 26, 2024 Published: April 5, 2024





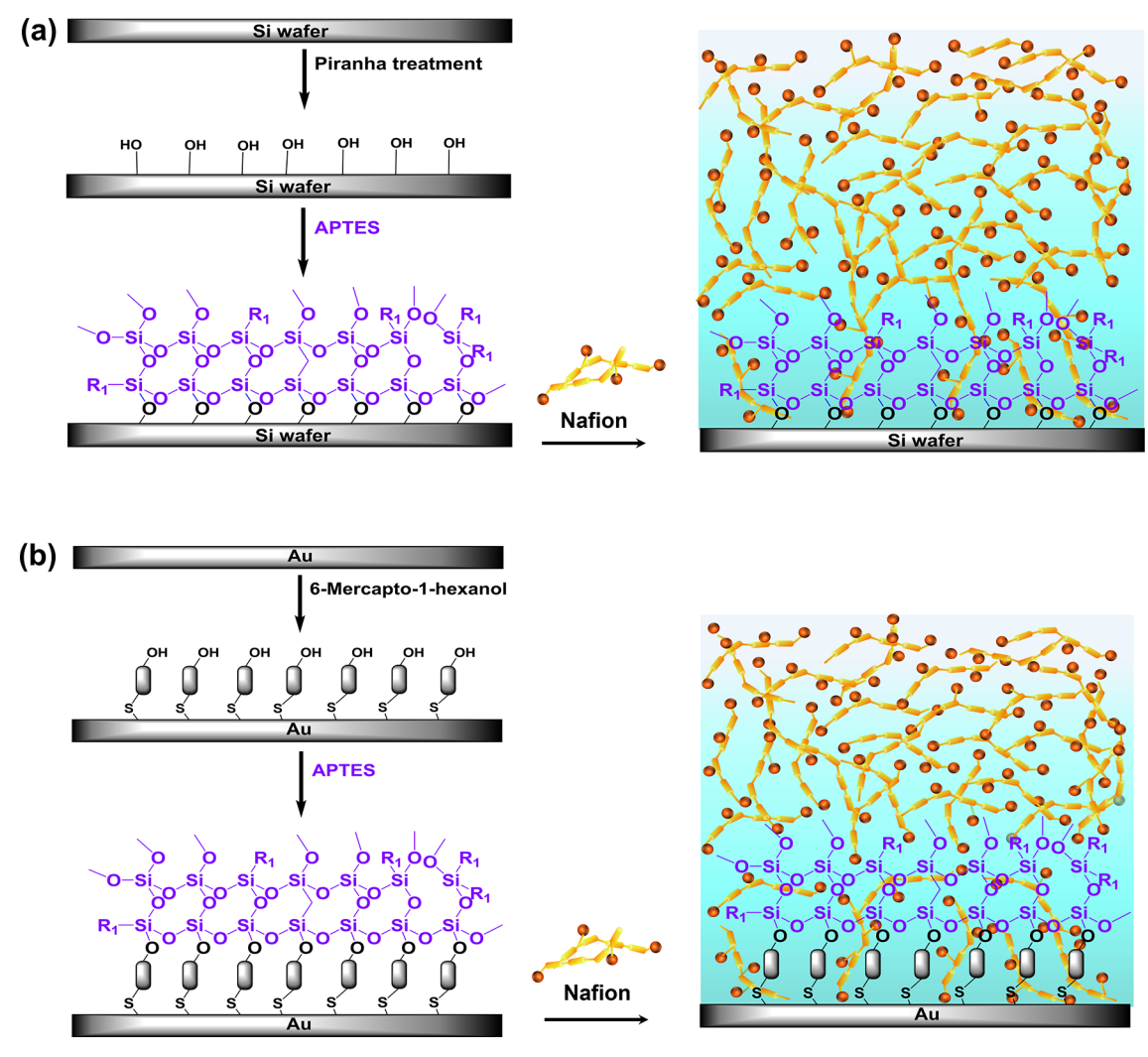


Figure 1. Schematics of self-assembly of APTES onto (a) silicon wafer or glass (-SiOH) and (b) Au IDE. After silanization of the surfaces (-SiOH or Au), Nafion thin films (blue-gray box) were deposited on top of them. The perfluorinated backbones of Nafion chains in the films are represented by orange-yellow chains, while the red balls represent terminal sulfonic acid ( $-SO_3H$ ) groups on the side chains appended to Nafion backbones.  $R_1$  shown in the silane structure represents ( $CH_2$ )<sub>3</sub>NH<sub>2</sub>.

substrate, 7,14,28-30 lose mobility, 7,14,20,31 and stiffen the films. 7,14,28,32,10 Interfacial effects around the substrate can also cause a distribution of glass transition temperature, 33-35 polymer chain dynamics, <sup>36,34</sup> mobility, <sup>9,20</sup> hydration, <sup>20,21</sup> and ion-conduction environment across ionomer films. 9,10,16,37-40 For example, using confocal laser scanning microscopy (CLSM), we are the first to reveal that ionic conduction across ionomer thin films varies along the depth of the film and is highly interface dependent.<sup>9,10,37</sup> Precisely, proton conduction of Nafion thin films on unmodified glass substrates was extremely weak over a broad region next to the substrate interface and then gradually ramped up as we approached the air interface. CLSM also identified a stiffened region next to the substrate within these Nafion films. This is unlike freestanding, bulk Nafion membrane which did not antiplasticize.<sup>7</sup> Also, the conductivity of bulk Nafion membrane was consistently high across the membrane. These observations on distributed properties again pointed toward the critical role played by interfacial processes and interactions in thin ionomer films. A similar conclusion was drawn by others 38,41,42 as the highly oriented lamella of ionomers or block copolymers near the electrode interface suppressed the through-plane ionic

conductivity in thin films. The surface-parallel ionomer chains adsorbed onto catalyst particles also made ORR active sites inaccessible to  $\rm O_2$  and caused performance loss of PEMFCs.  $^{10,43,30,44,45}$ 

To address these interfacial weak ion and gas transport issues within ionomer thin films, attempts have been made to alter the structure and chemistry of catalysts 46,26,47 and ionomers. 10,31,37,48 Interfacial restructuring is emerging as a promising approach to negate interfacial chain pinning and its detrimental effects (catalyst poisoning and slow ORR). For example, modifying the electrocatalysts with an inert skin layer, 46 rendering substrates with hydrophobic 26,49-51/electrostatically repulsive moieties, 26 or favorably orienting the lamellar structure<sup>38,42</sup> weakened the specific adsorption of -SO<sub>3</sub> anions of Nafion chains onto the substrate 46,26 and increased the overall proton conductivity  $^{26}$  as well as ORR activity. When ionic liquids (ILs),  $^{51-54}$  IL-modified block copolymers, 55,56 or peptides 43,57 were present at the catalyst active sites, phase segregation<sup>57</sup> and specific adsorption of ionconducting groups of ionomers on Pt altered in a manner which favored ORR and O<sub>2</sub> transport<sup>54</sup> in some cases.

While these studies shed light on surface modification effects, many fundamental questions persist regarding our understanding of ionomer films on engineered substrates. First of all, interface- and depth-specific information on proton conduction is largely missing in existing literature that explored the effects of interfacial engineering. We still do not know how the interfacial effects propagate across ionomer thin films on engineered substrates, whether the interfacial engineering manipulates the distribution of proton conduction behavior at different depths within the films, and, if yes, how. Furthermore, exploring depth-/interface-specific ion conduction behavior is crucial, alongside investigating other relevant aspects. For example, pure Nafion films on unmodified substrates showed weak next-to-substrate proton transport,9 while some other ionomers with varied molecular geometry and self-assembly capabilities (we recently reported 10,31,37,58) showed a boost in next-to-substrate proton transport. From these stemmed the idea that a porous or brush-like/spiderweb-like architecture adjacent to a substrate may prevent the surface-parallel alignment and anchoring of ionomers and facilitate proton conduction. Moreover, substrate hydrophobicity<sup>26,49-51</sup> and the number of surface-interacting functional groups of ionomers (-SO<sub>3</sub>H in Nafion) localized next to a substrate may determine the extent to which water and ionomer chains can be confined to the substrate. 10 These observations hinted that through interfacial engineering we can manipulate, understand, and make ionomer self-assembly, ionomer chain orientation, distribution of ionomeric functional groups, and mechanical properties of ionomer thin films more favorable for interfacial- and across-the-film proton conduction. Prior works have addressed one or a few of these aspects but not all. It is thus rational and critical to start with a simple yet effective surface engineering approach, build an extensive platform to deeply understand the interfacial processes, and then gradually proceed toward more complex interfacial systems leveraging the platform.

Keeping all of these in mind, here, we present a simple and robust electrode engineering approach that can easily manipulate the physical—chemical makeup of the ionomer—catalyst/substrate interface, alter the anisotropy within Nafion thin films, and improve interfacial and across-the-film proton conductivity.

The work presents a proof of concept where we engineered the substrate (SiO<sub>2</sub>, Au) interfaces first with (3-aminopropyl)-triethoxysilane (APTES) and then deposited sub- $\mu$ m-thick Nafion films on top (Figure 1a,b). Covalently immobilizing APTES at the ionomer—electrode interface enabled us to (i) disrupt the interfacial packing, pinning, orientation, and distribution of Nafion chains, (ii) narrow down the weak-proton-conducting zone next to substrate interface, and (iii) boost both in-plane and out-of-plane proton conductivity across Nafion thin films. Silanization is a simple and widely accepted surface engineering approach, but silanes anchored and localized next to the substrate may ensure selective positioning of Nafion chains next to the substrate as well as across the films.

We also established a holistic platform to understand the observed improvement in the proton conductivity within Nafion films on silanized surfaces. While electrochemical impedance spectroscopy (EIS) provides the average value of proton conductivity, it lacks the ability to reveal depth-specific ion-conduction behavior across ionomer thin films. Leveraging a CLSM-based strategy developed earlier, we captured this

crucial information, mapping the proton conduction environment across the film thickness. We integrated this depth-specific information with orientational and chemical makeup and mechanical properties of the films, which helped to understand the EIS data. Our simple yet effective silane-based interfacial engineering approach holds promise for guiding the reproducible, scalable design of interfaces/electrodes stable in a PEMFC microenvironment. Additionally, the platform we developed to deeply understand interfacial effects on overall and distributed properties within ionomer thin films can benefit the broader electrochemical research community working on diverse ionomer—catalyst interfaces.

#### MATERIALS AND METHODS

**Materials.** A 20 wt % Nafion solution (EW ~ 1100, IEC 0.909 mequiv/g), 6-mercapto-1-hexanol, and the photoacid probe (8-hydroxypyrene-1,3,6-trisulfonic acid trisodium salt (HPTS)) were purchased from MilliporeSigma (Milwaukee, WI). (3-Aminopropyl)-triethoxysilane (APTES) was purchased from Gelest Inc. (Morrisville, PA). Acetone was purchased from Fisher Scientific. Ethanol (anhydrous, denatured) was obtained from Decon Laboratories, Inc. (King of Prussia, PA). Silicon wafers coated with native silicon dioxide (SiO<sub>2</sub>) (thickness of native oxide layer ~ 1.72–1.79 nm) were purchased from Wafer Pro (San Jose, CA). Microscope coverslips (75 × 25 mm, thickness 170 μm) were purchased from ibidi USA, Inc. (Fitchburg, WI). Au interdigitated electrodes (IDEs) used for inplane proton conductivity measurements were obtained from Revtek Inc. (Torrance, CA).

Methods. APTES Self-Assembly on SiO<sub>2</sub> Wafer/Glass Substrate. For confocal laser scanning microscopy (CLSM), grazing incidence small-angle X-ray scattering (GISAXS), energy dispersive X-ray scanning electron microscopy (EDX-SEM), contact resonance atomic force microscopy (CR-AFM), and birefringence measurements, we created a layer of silane (APTES) on silicon wafers or glass slides (Figure 1a). The protocol for APTES self-assembly was similar to what was reported by others. 59,60 Briefly, prior to silane immobilization, the substrates were first "washed" with acetone and ethanol and air-dried. Thereafter, substrates were immersed in "Piranha" solution (75% H<sub>2</sub>SO<sub>4</sub>:25% H<sub>2</sub>O<sub>2</sub>) for 1 h. Caution: Piranha solution is a strong oxidizer and extremely corrosive in both liquid and vapor form. After piranha treatment, the substrates were rinsed copiously three times (40 s for each rinse) with DI water and dried under a stream of N<sub>2</sub>. Just before the silanization, the substrates were immersed for 5 min each in methanol, methanol:toluene (1:1), and toluene solutions, respectively. Next, the substrates were immersed in a 2% (v/v) APTES solution in toluene (stirred at 60 rpm) for a duration of 2 h for surface immobilization of APTES and to create an aminosilaneterminated SiO<sub>2</sub> wafer or glass substrate. After the reaction was complete, the silane-modified substrates were rinsed with toluene (10 min), methanol:toluene (1:1) (5 min), and methanol (5 min) to remove the unreacted silanes from the surface. The APTESterminated substrates were dried under a N2 stream and stored in a custom-built desiccated chamber for subsequent ionomer thin film deposition. Keeping the silane-terminated substrates in dry conditions is extremely critical as the silane layers are highly moisture sensitive. Also, for the best results, the APTES termination reaction should be performed in a well-ventilated fume hood or in a glovebox. The above-mentioned procedure yielded an APTES layer with thickness ~ 9-12 nm.

APTES Self-Assembly for EIS Measurements. EIS measurements had to be performed using Au-based electrodes. However, the geometry of the electrodes was different for in-plane and out-of-plane conductivity measurements. For the out-of-plane proton conductivity measurements, first, a narrow Au bar-electrode (3 mm  $\times$  3 mm) was deposited on a silicon wafer (with a Ti-adhesion layer in between the Au electrode and SiO<sub>2</sub>) after which the Nafion thin film was deposited. Finally, the second Au bar electrode was deposited on top of the Nafion layer. In out-of-plane geometry, the Nafion film

interfaced with  $SiO_2$  mostly. That is why, for the out-of-plane conductivity measurements, silanizing only the  $SiO_2$  regions of the substrate (not the Au bar electrode parts) was enough to see the silane effect on the Nafion films.

However, to see the effect of silane on Nafion films during the traditional in-plane proton conductivity measurement, we had to silanize the Au interdigitated electrodes (IDEs) (Figure 1b). In the inplane geometry, Au IDEs lay flat in an interdigitated manner on top of a silicon wafer (SiO $_2$ ) and thus occupied a distinct surface area of the substrate with which Nafion films can make contact. Therefore, silanizing could technically be done on either the Au or SiO $_2$  part of the substrate to see the effect.

Initially, we tried several approaches that had a close resemblance to what we followed to silanize glass/-silicon wafers. However, none of these results appeared to be effective. Since the Au layer is sensitive to piranha and silanization of silicon requires a piranha treatment (to increase the surface density of reactive hydroxyl groups on silicon), when we spin-coated the photoresist layer on SiO2, masked, UV treated, and then did piranha treatment (for subsequent silanization), the photoresist patterns got washed off. In the second attempt, we piranha-treated SiO<sub>2</sub> first and then tried to create the photoresist layer, mask, and UV treat. However, the formed photoresist patterns on the surface appeared to be disjointed. Using such a distorted photoresist layer yielded defective Au IDEs. In the third approach, when we spin-coated the photoresist layer, exposed it to UV with a mask on it to create a photoresist pattern, deposited a Ti (adhesion layer) and Au layer over the photoresist pattern, washed it with solvent (to remove the residue of the photoresist), and then treated it with piranha to modify the exposed SiO2 regions between IDE teeth for subsequent reaction with APTES, IDE performance dropped; i.e., proton conductivity of Nafion films on these IDEs was lower than Nafion films on regular Au IDEs. Lastly, when we tried to leverage the natural -OH functionalities of the silicon wafer (i.e., without trying the piranha treatment) to immobilize APTES, silanization was inefficient (as per XPS studies).

Therefore, to retain both the integrity and functions of Au IDEs while having a sufficient molecular density of APTES, we decided to silanize the Au surfaces instead of SiO<sub>2</sub> surfaces to prepare samples for in-plane proton conductivity measurement. We used a thiol-based cross-linker, 6-mercapto-1-hexanol, first to leverage Au-thiol affinity and create sufficient -OH terminals on the IDE surface, 61 followed by silanization as depicted in Figure 1b. Briefly, the IDEs were washed with acetone followed by ethanol and then UV-ozone cleaned (10 min). The IDEs were then dipped in a 5 mM 6-mercapto-1-hexanol solution in ethanol for 30 min. After the reaction, the IDEs were rinsed with ethanol thrice to remove unreacted 6-mercapto-1-hexanol. Subsequently, the IDE was dipped in a 2 v/v% APTES solution in toluene (stirred at 60 rpm) for 2 h. The silane-modified Au IDEs were rinsed with toluene (10 min), methanol:toluene (1:1) (5 min), and methanol (5 min). This approach of creating an APTES layer on Au IDE parts rather than on SiO<sub>2</sub> regions was efficient and bypassed the need for piranha treatment. Also, the 6-mercapto-1-hexanol layer on Au was very thin (<2 nm), and the APTES layer was of similar thickness (~10 nm), making the comparison of in-plane conductivity data with other measurements (where -SiOH was silanized instead of Au) reasonable.

Please also note that silanization of  $SiO_2$  required piranha treatment, but since the Au-bar electrodes (for out-of-plane measurement) were much wider than the teeth of Au IDEs (for in-plane measurements), we were able to maintain functional Au-bar electrodes, giving reliable out-of-plane proton conductivity data.

Thin-Film Preparation. A 20 wt % Nafion stock solution was diluted to 2–10 wt % using ethanol to prepare the thin films. Diluted samples were first vortexed and sonicated for  $\sim$ 15 min. The Nafion solutions were then directly spin-coated on the appropriate substrates (silane-modified or unmodified) using a spin coater (Headway Research, Inc., Garland, TX). The spinning was performed at 3000 rpm for a duration of 40 s. The spin-coated samples were dried for 3 h at 42 °C, annealed at 100 °C for 7 h, and cooled to room temperature overnight inside a vacuum oven (Model #1415, VWR, Radnor, PA).

Contact Angle Measurements. The water contact angle (WCA) of the substrates (before and after silane modification) and Nafion films were measured using a goniometer (Ramé-Hart Model 590 F4 Series Goniometer and Tensiometer). The sessile drop method was employed with 5  $\mu$ L of water dropped on the substrates and ionomer films, and a digital photograph of the system was taken to accurately measure the WCA. Figure 2 illustrates the WCA data obtained for

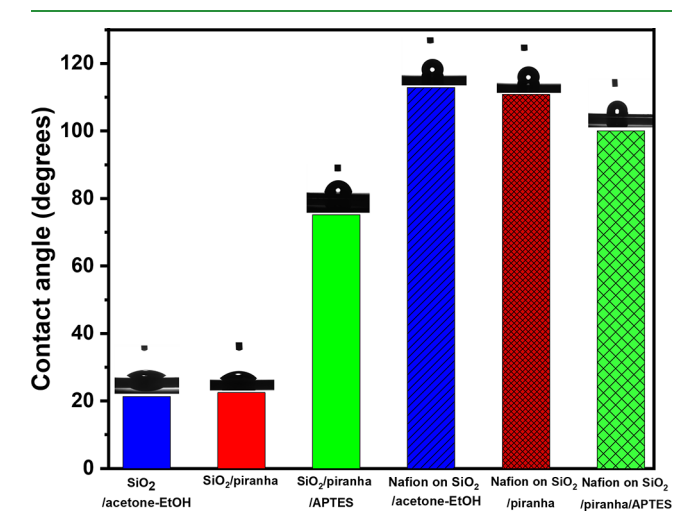


**Figure 2.** Sessile water contact angles of bare silicon wafers and the air interface of Nafion films before and after silane modifications.

 ${
m SiO_2}$  surfaces treated with various methods and Nafion films on those, while Figure S1 shows analogous data for differently treated Au surfaces.

Confocal Laser Scanning Microscopy (CLSM). For CLSM imaging, the ionomer films were prepared following a similar protocol we described in prior work. <sup>9,37</sup> Briefly, coverslips ( $75 \times 25 \times 170 \,\mu\text{m}$ , ibidi USA, Inc., Fitchburg, WI)) were washed with acetone and ethanol and then treated with UV-ozone for 20 min. A solution of Nafion containing 0.75 mM HPTS (Figure S2a) was spin-coated at 3000 rpm for 40 s on the cleaned and UV-ozone-treated coverslips. The thickness of the HPTS-stained ionomer films (~60 nm, ~250 nm, and ~650 nm) was controlled by controlling the wt % of ionomer (2, 7.5, and 10 wt %) in solution. The films were dried under vacuum for 3 h at 42 °C, annealed at 100 °C for 7 h, and then cooled to room temperature overnight. The samples were stored in desiccated plastic containers wrapped with aluminum foil and taken to the CLSM facility for imaging. Using an ibidi humidifying system (ibidi USA, Inc., Fitchburg, WI), the samples were equilibrated at 90% RH inside an in situ environmental chamber, which was placed under the microscope. The humidification chamber and imaging setup are shown in our prior work.9

Nikon-Ti2 inverted fluorescence microscope with a Nikon NIS Element-C image acquisition program (Nikon Corp, USA) was used for all CLSM imaging. Emission data were collected with laser lines 405 and 488 nm and a  $20\times$  dry lens. The system was also set to a *z*-interval of 100 nm between *xy*-plane images for relatively thicker films (250–700 nm thick Nafion films). For the very thin films we studied (e.g., 60-70 nm thick), we focused on the topmost and bottommost fluorescent *xy*-planes, the emission intensities of which gave a HPTS response at the air and substrate interfaces of those films, respectively.

In-Plane Proton Conductivity Measurements. The proton conductivity values of ionomer thin films were measured using electrochemical impedance spectroscopy (EIS) (Solartron 1260a Impedance/Gain-Phase analyzer attached to the Solartron 1296 Dielectric Interface (AMETEK Scientific Instruments, Berwyn, PA)) via a 2-probe technique over 10 MHz–10mHz frequency range at 100 mV AC potential. To rin-plane proton conductivity measurements, ionomer films were spin-coated on unmodified and APTEsmodified Au IDEs. The Au IDEs were deposited on top of a silicon

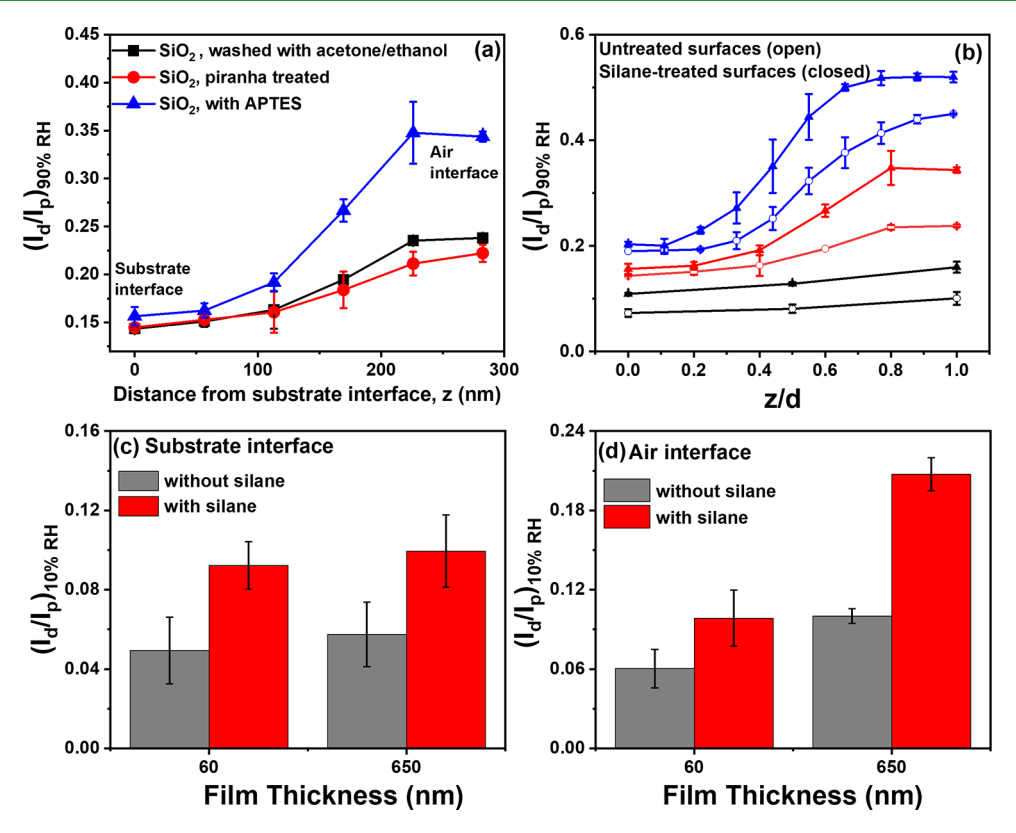


Figure 3. (a)  $I_d/I_p$  profile (extent of proton conduction) at 90% RH of ~250 nm-thick annealed Nafion films on glass substrates before and after silanization. (b)  $I_d/I_p$  profile of Nafion thin films (~60 nm (black), ~250 nm (red), and ~650 nm (blue)) as a function of film thickness. Open symbols represent Nafion films on untreated SiO<sub>2</sub> surfaces (just washed with acetone/ethanol), while closed symbols represent Nafion films on silane-treated SiO<sub>2</sub> surfaces at 90% RH. In (b), the thickness-normalized distance from the substrate is represented by z/d, where z is the distance from the substrate interface and d is film thickness. Therefore, z/d values of 0 and 1 represent the substrate and air interfaces of the films, respectively. (c, d)  $I_d/I_p$  values at 10% RH for ~60 and ~650 nm-thick annealed Nafion films at the air and substrate interfaces on both untreated (grey) and silane-treated (red) surfaces. Measurements were done in triplicate, and error bars were calculated based on standard deviations.

wafer having a 200 nm thermal oxide layer on it. The IDEs were purchased from Revtek Inc. (Torrance, CA). Each IDE had 150 gold teeth (N) where the width of a single tooth (w) was 8  $\mu$ m and the gap between two teeth ( $S_{\rm teeth}$ ) was 40  $\mu$ m. The overlapping length of the teeth (1) was 4 mm. For effective APTES immobilization on the Au IDEs, a thiol-based cross-linker, 6-mercapto-1-hexanol, was first used to form -OH terminals on the IDE surface, 61 followed by the silanization strategy described in Figure 1b and APTES self-assembly section. Ionomer solutions were then deposited on unmodified and APTES-modified IDEs, dried, and annealed. Prior to the measurements, the contact pads were cleaned (with ethanol). Ionomer-coated IDEs were then placed in the measurement chamber and exposed to different relative humidities (~25% and ~85% RH). The humidity inside the chambers was maintained using the appropriate saturated salt solutions. All samples were equilibrated at each %RH for at least 1 h. During humidification, the samples were checked by a shortfrequency measurement (1-10 kHz range) to ensure the stability of the system. Fitting information on in-plane proton conductivity data and representative fits can be found in Figure S3.

Out-of-Plane Proton Conductivity Measurements. Out-of-plane proton conductivities of Nafion thin films on SiO<sub>2</sub> wafers and silane-modified wafers were measured following a specific experimental procedure outlined in the literature.  $^{37,42}$  To create the EIS sample, a silicon wafer with a 200 nm thermal oxide layer was used as a substrate. Briefly, a 50 nm-thick Au bar-electrode (3 mm long × 3 mm wide) was deposited on this SiO<sub>2</sub> wafer with a Ti-adhesion layer (3 mm × 3 mm) in between Au and SiO<sub>2</sub>. These depositions were carried out using a mask and an ATC-2000F sputtering system from AJA International (Scituate, MA). Nafion film was deposited on this substrate with the Au bar electrode and annealed subsequently. Finally, the second Au bar electrode was deposited on top of the

annealed Nafion layer. This produced out-of-plane EIS samples of Nafion films on unmodified substrates. We also made out-of-plane EIS samples of Nafion films on silanized substrates. Please note that, if we just silanized the tiny Au bar electrodes (leaving the majority  $\rm SiO_2$  region, in touch with Nafion film, not silanized), the silanization effect on the Nafion film would have been so negligible that it could not be captured in the out-plane conductivity. This is why, to see the effect of silane on the out-of-plane conductivity of a Nafion film, the  $\rm SiO_2$  region of the wafer (having an Au bar electrode at one edge) was silanized (following the protocol described earlier in APTES self-assembly on  $\rm SiO_2$  wafer section). Subsequently, the Nafion layer and a second Au bar electrode were deposited. The out-of-plane ionic conductivity ( $\sigma_{\rm OP}$ ) of the samples was then measured using the Solartron system at  $\sim$ 83–86% RH. Representative fits are shown in Figure S4.

#### ■ RESULTS AND DISCUSSION

In this work, to study the effect of interfacial engineering, we deposited  ${\sim}60{-}600$  nm thick Nafion films on APTES-terminated model substrates. When silicon wafers or glass slides (SiO<sub>2</sub>) were used as substrates, we first covalently immobilized (3-aminopropyl)triethoxysilane (APTES,  ${\sim}9{-}12$  nm thick) on the substrate. Subsequently, Nafion films were spin-coated on top of these APTES-terminated substrates (Figure 1a). We created this ensemble for confocal laser scanning microscopy (CLSM), grazing incidence small-angle X-ray scattering (GISAXS), energy dispersive X-ray scanning electron microscopy (EDX-SEM), contact resonance atomic force microscopy (CR-AFM), birefringence, and out-of-plane

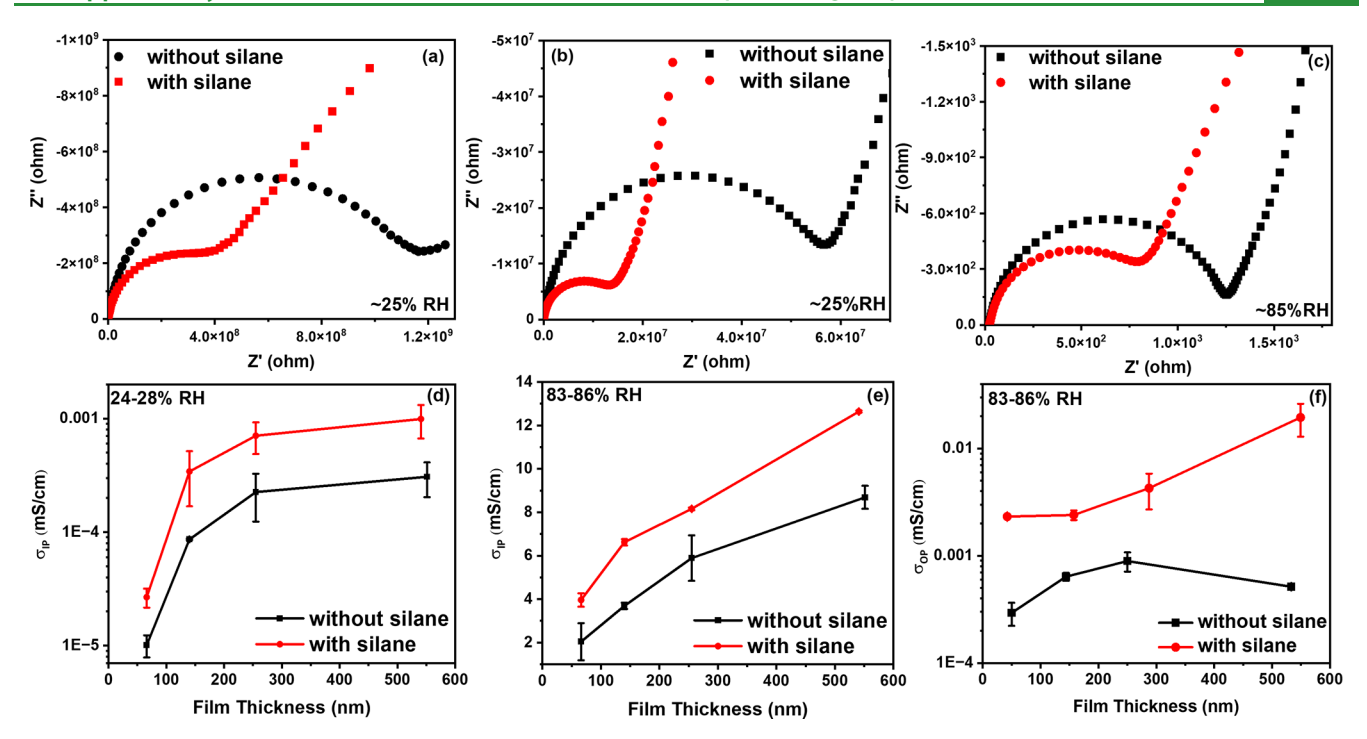


Figure 4. In-plane Nyquist plots of (a)  $\sim$ 60 nm Nafion films at 25% RH, (b)  $\sim$ 140 nm Nafion films at 25% RH, and (c)  $\sim$ 140 nm Nafion films at 85% RH on untreated and silane-treated Au interdigitated electrodes (IDEs). (d, e) In-plane conductivity and (f) out-of-plane conductivity of Nafion films on untreated and silane-treated surfaces at low (d) and high (e, f) humidity conditions as a function of film thickness. Measurements were done in triplicates, and error bars were calculated based on standard deviations.

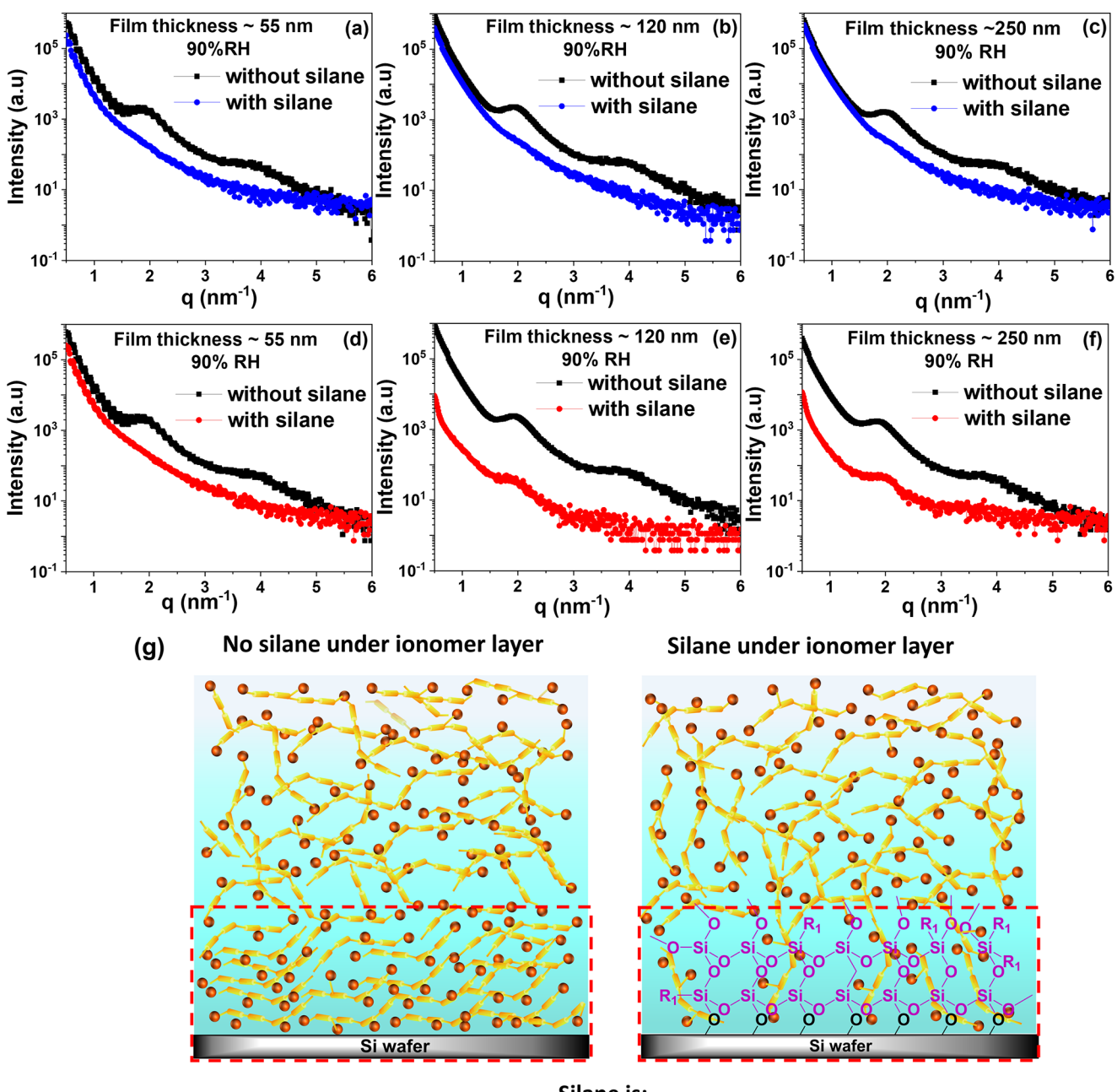
proton conductivity measurements. On the other hand, for the in-plane proton conductivity measurements, Nafion films were spun on Au interdigitated electrodes (IDEs) where the teeth Au IDEs were evenly spaced across the silicon wafer. Thus, to create a similar silane environment on Au IDEs to match other measurements, we immobilized silane on the Au part. First, the Au-thiol interaction was leveraged between Au IDEs and a thiol-functionalized compound, 6-mercapto-1-hexanol (Figure 1b). This created —OH terminated Au, which reacted further with APTES (Figure 1b). Please see the APTES self-assembly section in the Methods section for further details.

Silanization of the substrates was confirmed by using X-ray photoelectron spectroscopy (XPS, Table S1). The water contact angles (WCAs) of bare SiO<sub>2</sub> surfaces after washing with acetone (21°), treating with piranha (23°), and immobilizing APTES (75°) (Figure 2) showed that silanization reduced the hydrophilicity of the bare substrate. The significant change in the water contact angle upon silanization of silicon wafer agreed with the data reported by other groups. 59,60 When Nafion was deposited on these three surfaces, the WCA was the lowest (i.e., lowest hydrophobicity) for the film on the silanized surface. These suggested that the APTES modification of SiO<sub>2</sub> significantly altered the hydrophilicity of both substrate and air interfaces of Nafion films. Silanization also reduced the hydrophilicity of Au surfaces (28° (Au with MHex), 47° (APTES on Au with MHex), Figure S1). The decreased hydrophilicity of the substrate interface as a result of silanization is likely to dictate how the - SO<sub>3</sub>H groups of Nafion side chains sit and interact with the substrate.

To see the impact of the silane layer on the distribution of the proton conduction environment at different depths within Nafion films, we leveraged our CLSM-based strategy (Figures 3 and S2). 9,10,37 A fluorescent photoacid dye (8-hydroxypyrene-1,3,6-trisulfonic acid trisodium salt (HPTS), Figure S2a)

was added to the Nafion suspension before spin-coating it over silanized/non-silanized substrates. HPTS remains protonated and emits blue fluorescence ( $I_{\rm p}$ ,  $\lambda_{\rm em} \sim 430$  nm) when it resides in a poorly proton-conducting environment. On the contrary, the dye emits green fluorescence upon deprotonation ( $I_{dr}$   $\lambda_{em}$  $\sim$  510 nm) in a stronger proton-conducting environment. The ratio of green-to-blue fluorescence  $(I_d/I_p)$  at different depths within Nafion films can thus reveal the extent of proton conduction across the films.<sup>9,10,37</sup> It is important to recognize that  $I_d/I_p$  refers to the "extent of proton conduction", a qualitative measure of proton conductivity, as opposed to the quantitative measurements of proton conductivity  $(\sigma)$ , typically done using EIS. It was demonstrated earlier that  $\sigma$ and  $I_d/I_p$  provide complementary information. The advantage of the fluorescence CLSM-based technique is that it can be leveraged to get information on proton conduction at different depths within an ionomer film, while EIS only provides an average value of proton conductivity for the entire ionomer film.

Figure 3a shows proton conduction profiles (represented by  $I_{\rm d}/I_{\rm p}$ ) of ~250 nm thick Nafion films as a function of distance from the substrate interface (z). When Nafion films were deposited on non-silanized surfaces with similarly high hydrophilicity (i.e., SiO<sub>2</sub> washed with acetone/ethanol or piranha-treated), the proton conduction profile of the ionomer films looked similar. Briefly, the substrate interface of these Nafion films had a weak proton-conducting zone ( $I_{\rm d}/I_{\rm p}\sim0.14$ , Figure 3a). After that, the  $I_{\rm d}/I_{\rm p}$  increased gradually (~0.23) as we approached the air interface, suggesting a relatively better proton conduction environment at the air interface as compared to the substrate interface. Interestingly, when we had a silane layer (APTES) underneath the Nafion film, the low-conductivity region next to the substrate interface shortened and proton conduction at the air interface



Silane is:

likely letting lesser number of chains reach to substrate interface
 suppressing the lamellar chain orientation
 reducing interfacial interaction effect

Figure 5. (a–f) GISAXS profiles of Nafion films on unmodified and APTES-modified substrates at 90% RH. To do these measurements, (a–c)  $\theta/2\theta$  and (d–f)  $\omega/2\theta$  scanning geometries were used. Here, the dry Nafion film thicknesses were (a, d) ~55 nm, (b, e) ~120 nm, and (c, f) ~250 nm. (g) Schematic representation of the possible effect of silanization on the Nafion chain orientation next to the substrate. The Nafion film is represented by a bluish-green box with orange-yellow Nafion chains having red balls as terminal  $-SO_3H$  at the side chains. The APTES structure is shown in purple. The red dotted box indicates the region next to the substrate where silane may alter the traditional lamellar structure in Nafion films.

significantly improved  $(I_{\rm d}/I_{\rm p}\sim 0.35,$  Figure 3a). Such improvement in proton conduction within Nafion films over the silanized substrate was observed for the entire film thickness range we studied (60–700 nm, Figure 3b). An  $\sim$ 650 nm thick Nafion film with no silane underneath had a weakly proton-conducting region spanning up to z/d of 0.3; i.e., up to one-third of the film starting from the substrate interface. However, when Nafion was deposited on the

APTES-treated surface, the weakly proton-conducting region narrowed down to  $z/d \sim 0.1$  (Figure 3b). Moreover, the extent of proton conduction  $(I_{\rm d}/I_{\rm p})$  across the films on silane-treated surfaces improved irrespective of film thickness; e.g.,  $I_{\rm d}/I_{\rm p}$  at the air interface of a 250 nm thick Nafion film increased from 0.19 to 0.35 when a silane layer was underneath the film (Figure 3b). Such improvement of ion conduction environ-

ment across Nafion films on silane was observed at both high (Figure 3b) and low (Figure 3c,d) humidity conditions.

Typically, hydrophilic surfaces (like SiO<sub>2</sub>) attract and pin -SO<sub>3</sub>H groups of Nafion via hydrogen bonding, inducing a surface-parallel orientation of Nafion chains near the substrate. 21,23,29,62 The thickness of this multilamellar region  $(\sim 10 \text{ nm})$  is comparable to that of our silane layer. Simulations indicated that highly hydrophilic surfaces retain water molecules next to them but hydrophobic surfaces promote the presence of hydrophobic components like the Nafion backbone. Our silane treatment reduced the hydrophilicity of the SiO<sub>2</sub> substrate which likely pushed the water and -SO<sub>3</sub>H groups of ionomer chains away from the substrate. The spider web/brush-like structure of the silane layer also hindered the contact of hydrophobic Nafion backbones with the substrate interface. This low hydrophilicity and unique silane structure minimized the substrate-induced entrapment of Nafion chains and water molecules, thereby improving proton conduction in the Nafion films. These findings align with previous research showing that introducing hydrophobic or electrostatically repulsive functionalities can prevent specific adsorption of -SO<sub>3</sub> ions of Nafion onto catalysts and improve proton transport and ORR activity. 26,51-53

We further quantified the ionic conductivity of Nafion films on Au electrodes using EIS which supported our observations using CLSM. The procedures for APTES immobilization on Au-interdigitated electrodes (IDEs) are available in Figure 1b and in the Methods section. The film resistance in the in-plane Nyquist plots (equivalent to the diameter of the semicircular region of the impedance curves) decreased when there were silane layers underneath the Nafion layers (Figure 4a-c). The equivalent circuit model (Figure S3a) was used to fit the inplane Nyquist plots, and some representative fits of the inplane impedance curves (Figure S3b,c) to obtain in-plane proton conductivity ( $\sigma_{IP}$ ) values are shown in the Supporting Information. The decreased film resistance indicated that the ionic conductivity ( $\sigma_{IP}$ ) increased in Nafion films when they were spin-coated on APTES-terminated substrates. To understand the contribution of silane relative to Nafion in this film proton conductivity, we compared the Nyquist plots of bare Au IDE, silane on Au IDE (Au IDE/silane), and a Nafion film over silane (Au IDE/silane/Nafion) (Figure S5). As per the visual inspection of these Nyquist plots, the diameters of the semicircles for Au IDE and Au IDE/silane were so large that those could not be captured fully by the EIS instrument, while the Au IDE/silane/Nafion film ensemble gave a reasonable and measurable diameter of the semicircle (Figure S5). This control experiment suggested that silane itself had a negligible proton conductivity as compared to Nafion films and thus made a negligible contribution to the overall proton conductivity of the Nafion-on-silane samples. Despite this, the heightened proton conductivity of Nafion films on APTEStreated surfaces (Figure 4) suggested that the silane layer might have made a profound impact on Nafion layer characteristics (discussed later).

Silanization-induced improvement in proton conductivity of Nafion films was observed at both low (25% RH, Figure 4b,d) and high (85% RH, Figure 4c,f) humidity conditions irrespective of film thickness. The improvement in in-plane proton conductivity ( $\sigma_{\rm IP}$ ) at low %RH (~3 times, Figure 4d) agreed with CLSM data where the Nafion films on silane showed  $I_{\rm d}/I_{\rm p}$  values ~2 times higher than that of Nafion films on untreated substrates (Figure 3c). In fact, the CLSM and EIS

data agreed well across the entire relative humidity (%RH) range (Figure S6). Not only that, both in-plane ( $\sigma_{IP}$ , Figure 4d,e) and out-of-plane (( $\sigma_{OP}$ , Figure 4f) conductivity values of Nafion films showed improvement on silane-treated surfaces; e.g., at ~83–86% RH, in 250 nm thick Nafion films, we obtained:  $\sigma_{IP}$ : 5 mS/cm (unmodified); 8 mS/cm (silane-modified) (Figure 4e);  $\sigma_{OP}$ : 8.93 × 10<sup>-4</sup> mS/cm (unmodified); 4.27 × 10<sup>-3</sup> mS/cm (silane-modified) (Figure 4f). Even in Nafion films with thickness (~60 nm) closer to catalyst binder layers in PEMFCs, we saw such silane-induced improvement in  $\sigma_{IP}$  (2 times) and  $\sigma_{OP}$  (10 times) (Figure 4e,f). It is well-reported that, for Nafion thin films on unmodified surfaces, in-plane proton conductivity is significantly higher than out-of-plane conductivity. We thus also made a similar observation for Nafion films on both unmodified and silane-modified surfaces.

Revisiting the discussion on how silane improved the Nafion film proton conductivity, we examined several factors. First, we examined the influence of silane on water uptake by Nafion films. However, when Nafion films were made on non-silanized and silanized Au QCM crystals, the average water uptake or hydration numbers  $(\lambda_w)$  did not appear to be much different (Figure S7). This observation directed attention to another prominent factor: the silane layer potentially modified the nanostructure of the Nafion layer, thereby affecting its enhancement in proton conductivity.

Silanization improved the in-plane  $(\sigma_{\rm IP})$  and out-of-plane  $(\sigma_{OP})$  proton conductivities of Nafion films. Also, it reduced the ratio of in-plane-to-out-of-plane proton conductivity ( $\sigma_{\text{IP}}$ /  $\sigma_{\rm OP}$ ) and led it to convergence toward unity (Figure 4e,f), a scenario where film nanostructure does not trigger directiondependent proton conductivity. Based on the improved conductivity and altered anisotropy in conductivity, we hypothesized that silanization of the substrate likely changed the organization of Nafion chains across the films and ultimately impacted the distribution of the ion-conduction environment across Nafion films. We, therefore, studied the grazing incidence small-angle X-ray scattering with a point detector (0D GISAXS) to see how silane modified the order within Nafion films (Figure 5). We performed a scattering study using both  $\theta/2\theta$  and  $\omega/2\theta$  geometries. While  $\theta/2\theta$ enabled us to capture the order or repeating structure in the zdirection,  $\omega/2\theta$  captured repeated structures in both z- and xydirections. In  $\theta/2\theta$  scans (Figure 5a-c), the primary ionomer peak for Nafion on an unmodified surface was seen at the same position as has been reported typically  $(q \sim 1-2 \text{ nm}^{-1})$ .<sup>63</sup> We also saw a secondary peak  $(q \sim 3-5 \text{ nm}^{-1})$  which has been reported by several groups. <sup>64,65</sup> Both of these peaks completely disappeared when Nafion films were on APTES-treated surfaces, irrespective of the film thickness (Figure 5a-c). Silanization did not only impact the out-of-plane order but also affected the in-plane order. In  $\omega/2\theta$  scans (Figure 5d-f), the orders were weakly retained in relatively thicker (120-250 nm thick) films with a slight shift in scattering peak. For example, for an  $\sim$ 250 nm thick Nafion film (Figure 5e),  $q_{\text{max}}$  for the primary ionomer peak was found to be ~1.86 nm<sup>-1</sup> (without silane) and 1.94 nm<sup>-1</sup> (with silane), which corresponded to the d-spacings of  $\sim 3.35$  nm (without silane) and 3.24 nm (with silane), respectively. While the scattering peak in thicker films (120-250 nm thick, Figure 5e,f) weakened in intensity but still remained, the scattering peak totally diminished in thinner films on silane (~55 nm, Figure 5d). This suggested

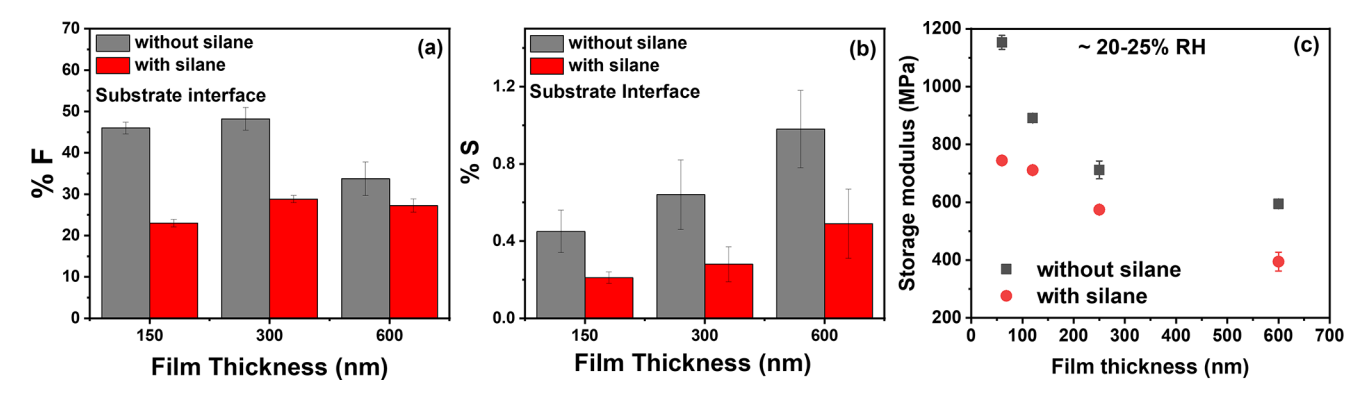


Figure 6. (a, b) SEM-EDX quantification near the substrate interface: (a) % F and (b) % S. (c) Storage modulus at ~20–25% RH of 50–600 nm-thick Nafion films on untreated and silane-treated surfaces, respectively. Measurements were done in triplicates, and error bars were calculated based on standard deviations.

that the orders completely disappeared in thinner films on silane.

Such disruption of ionic domains can be discussed in light of prior works on Nafion thin films. Typically, meaningful information on structural orders within ionomer thin films is obtained by using neutron reflectometry, 2D GISAXS, and simulation. For example, Weber et al.,3 via some advanced analysis of ionomer peak (as a function of azimuthal angle) using 2D GISAXS, suggested that Nafion and some other perfluorinated 3 M ionomers have preferential domain alignment parallel to the substrate in thin films. In another work, Kreuer et al.<sup>64</sup> simulated and compared the experimental GISAXS data within the 1-5 nm<sup>-1</sup> region for stacked planar polymer-water sheets. When some degree of disorder was introduced in such stacked structures, the diffraction peaks broadened, and good fits were obtained within this q-range. Finally, Dura and DeCaluwe pioneered neutron reflectometry work showing the location of the stacked structures within Nafion films. 21,29,42,47 They asserted the surface-parallel lamellar structure near the substrate interface of the Nafion thin films.

All of these studies suggested the likelihood of having stacked or lamellar structures in Nafion films on the unmodified substrate (Figure 5g, left). On the contrary, the loss of correlation in Nafion films on silane likely manifested an induced disorder in lamella and/or a randomization of ionomer chains in all directions (Figure 5g, right). As per neutron reflectometry,<sup>21</sup> the lamellar region usually spans around the 10 nm region within the film next to the unmodified surface. On the other hand, the thickness of our APTES layer was ~9-12 nm. This strengthened our hypothesis that silane has a contribution to disrupting or suppressing the surface-parallel lamella of Nafion chains (Figure 5g, right). If silane is suppressing the lamella formation by letting a lower number of chains reach the substrate interface, the ionomer-substrate interaction next to the substrate (Figure 5g, right) can be milder. This weakened interfacial interaction can be a major reason behind the improved conductivity<sup>7,26</sup> in ionomer films on silane. Literature on block copolymer thin films also supports how lamella weakens the ionic conductivity in the direction the lamella grows. 38,41,42 Therefore, the disruption of the lamella and significant improvement in through-plane proton conductivity in our case (Figure 4f) complemented each other.

On another note, our CLSM data suggested that ionic conductivity was not only getting better close to the APTES-

treated substrate interface but also improved throughout the Nafion films (Figure 3). This likely suggested that the silane layer, despite being next to the substrate, may impact the properties of the entire film. This is not uncommon. For example, Drummond et al. 66 discussed the structuration of the entire polymer thin film via controlled patterning of the supporting substrate. In fact, they showed that substrate pinning and unpinning can determine the mobility of polymer chains at the air interface. Thus, it can be rationally inferred that the reduced extent of interfacial chain pinning can be a major manipulator and booster of proton conductivity near the air interface (CLSM, Figure 3).

Since GISAXS hinted toward the disruption in ionic domains and lamellar chain packing in the presence of silane, an alteration of atomic composition next to the substrate can be expected. SEM-EDX supported so (Figures 6a,b and S8). Both %F (Figure 6a) and %S (Figure 6b), components of Nafion, decreased at the substrate interface as a silane layer was placed in between the Nafion film and SiO2. For example, in a 150 nm thick Nafion film, %F in a region next to the substrate interface with dimensions 75 nm (height)  $\times$  1350 nm (length) decreased from 46% to 23% as the silane layer was placed underneath the Nafion layer (Figures 6a and S8a,b). A simultaneous decrease in %S was also observed for Nafion films on the silanized surface (%S: 0.45% (no silane), 0.21% (with silane) for a 150 nm thick Nafion film, Figures 6b and S8). This suggested that the silane layer next to the substrate led to a reduced population of Nafion chains next to the substrate. Similar trends were consistently seen for Nafion films over the entire thickness range (150-600 nm) that we studied (Figure 6a,b). This supported our prior hypothesis and depiction of the silane effect (Figure 5g, right) that ionomer chains are likely finding it difficult to reach the substrate interface because of silane crowding at that location. Ionomer chain density next to the substrate thus decreased, and both backbone and side chains of Nafion were likely oriented differently when silane was there next to the substrate.

To understand the nature of the alteration in the orientation of ionomer chains with respect to the substrate, we measured the birefringence  $(\Delta n)$  of Nafion films with and without a silane layer underneath. To date, only a few reports have been made on  $\Delta n$  of ionomer thin films as a way to explain the orientation of ionomer backbones and respective side chains in ionomer thin films.<sup>24</sup> Conventionally, a birefringence less than zero represents the polymer backbones parallel to the substrate, while a birefringence value of zero indicates an

isotropic or random orientation of the backbones with respect to the substrate. We found that, for a pure Nafion film with no silane layer underneath,  $\Delta n$  was negative, but when a silane layer was placed underneath the Nafion layer,  $\Delta n$  approached zero (Figure S9). This, alongside the GISAXS and SEM-EDX data, confirmed that the silane layer initiated an alteration of the ionomer chain orientation in the films overall and led toward a more isotropic (randomized) chain structure. The randomization was done in such a way that favored proton conduction in thin films.

On another note, Nafion films are known to stiffen at low humidity conditions which is often attributed to interfacial interactions between  $-SO_3H$  groups of Nafion, substrate, and interfacial water. We thus measured the storage modulus of Nafion films at ambient conditions using CR-AFM. The storage modulus of a ~60 nm thick Nafion film on an unmodified substrate (~1100 MPa) was significantly higher than that for the Nafion film on an APTES-treated substrate (~800 MPa) (Figure 6c). While CR-AFM is a local modulus measurement technique, such a big decrease in the modulus of films with silane underneath demonstrated a critical role played by substrate and interfacial interactions on the modulus of the entire film. This together with the fact that the sulfur atoms are less reachable to the substrate interface suggested that the substrate pinning-induced film stiffening may have been alleviated by the presence of a silane layer next to Nafion film.10

In summary, in this work, we used APTES to demonstrate a proof of a concept; i.e., if you create a silane-like structure next to the substrate, you can boost thin-film proton conductivity. Not only did we demonstrate the utility of interfacial engineering through exploring depth-specific ion conduction behavior but also unraveled a wealth of information explaining why interfacial engineering improved next-to-substrate as well as across-the-film proton conduction properties. The major takeaway from this work in a broader sense is that, by creating hydrophobicity and/or brush/spider web-like architecture next to the substrate, we may be able to prevent some of the interfacial phenomena (like, chain pinning, lamella, interfacial confinement) detrimental for proton conduction in thin Nafion films (Figure 5g). Our vision was to harness the relatively less complicated silane platform to uncover a plethora of insights into the interfacial behavior of ionomer thin films, but the success of this APTES-based study suggested the importance of leveraging and building up on this platform via exploring a wide range of engineered interfaces and seeing their impact further in thin films, real electrodes, and membrane electrode assemblies. By exploring these avenues, we will continue to advance the concept further and inform the advanced design of ionomer-catalyst interfaces for an array of electrochemical systems.

### CONCLUSIONS

We demonstrated how through a simple surface engineering approach we can manipulate the interfacial orientational and chemical makeup that can make the overall proton conduction environment more favorable in sub- $\mu$ m-thick Nafion films. Introducing an APTES-based silane layer between the substrate and Nafion thin film disrupted the order/repeating structure within the Nafion film (GISAXS) and reduced the Nafion chain density next to the substrate (SEM-EDX). Especially, the suppression of surface-parallel lamella may have reduced substrate-pinning of ionomer chains and interfacial

confinement (reflected in birefringence and storage modulus). As a result of these modifications in the interfacial environment, the poorly proton-conducting region next to the substrate interface narrowed (CLSM) and made the proton conduction environment across the Nafion films become more favorable. The enhancement in the proton-conductive environment across the Nafion films induced by silane, as evidenced by CLSM, aligned with the improved proton conductivity (both in-plane and out-of-plane) observed in Nafion films through EIS. Overall, this work offers a promising pathway to overcome interfacial ion-transport limitations and elevates our understanding of the interfacial processes. In particular, the depth of insights into interfacial phenomena and the propagation of their effects uncovered in this study distinguish it as a unique contribution to the field. The established protocols offer valuable guidance for attaining greater control over interfacial processes in sustainable energy-driven electrochemical devices and for advancing our understanding of them.

# ASSOCIATED CONTENT

# Supporting Information

The Supporting Information is available free of charge at https://pubs.acs.org/doi/10.1021/acsapm.3c03218.

Thickness measurement, surface elemental analysis (XPS), CLSM, EIS, QCM SEM-EDX, birefringence, CR-AFM, and additional experimental details (PDF)

#### AUTHOR INFORMATION

## **Corresponding Author**

Shudipto Konika Dishari — Department of Chemical and Biomolecular Engineering, University of Nebraska-Lincoln, Lincoln, Nebraska 68588, United States; orcid.org/0000-0003-1679-2332; Email: sdishari2@unl.edu

#### Author

Oghenetega Allen Obewhere — Department of Chemical and Biomolecular Engineering, University of Nebraska-Lincoln, Lincoln, Nebraska 68588, United States

Complete contact information is available at: https://pubs.acs.org/10.1021/acsapm.3c03218

#### Notes

The authors declare no competing financial interest.

#### ACKNOWLEDGMENTS

The research was supported by the National Science Foundation (NSF) CAREER Award (NSF-DMR # 1750040). S.K.D. and O.A.O. also acknowledge partial support from the NSF-CBET#2310185 and U.S. Department of Energy (DOE), Office of Science, Basic Energy Sciences (BES) Early CAREER Award (#DE-SC0020336). Part of this research (XPS, SEM-EDS, GISAXS, birefringence) was performed in the Nebraska Nanoscale Facility: National Nanotechnology Coordinated Infrastructure and the Nebraska Center for Materials and Nanoscience, which are supported by the NSF under Award ECCS: 2025298 and the Nebraska Research Initiative. The microscopy work was carried out at the Morrison Microscopy Research Core Facility of the Center for Biotechnology, which is partially funded by the Nebraska Center for Integrated Biomolecular Communication COBRE grant (P20 GM113126 and NIGMS) and the Nebraska Research Initiative. S.K.D. and O.A.O. acknowledge the

guidance of You Zhou (UNL) in developing the CLSM protocols. The authors also thank the Nano-Engineering Research Core Facility (NERCF) at UNL for CR-AFM studies. O.A.O. acknowledges Ehsan Zamani for assistance with birefringence experiments and Henry Ems for the training in contact angle measurements. O.A.O. thanks Karen Acurio Cerda and Rajesh Keloth for help in drawing the schematics.

#### REFERENCES

- (1) Avid, A.; Zenyuk, I. V. Confinement Effects for Nano-Electrocatalysts for Oxygen Reduction Reaction. *Curr. Opin. Electrochem.* **2021**, *25*, 100634.
- (2) Wang, H.; Wang, R.; Sui, S.; Sun, T.; Yan, Y.; Du, S. Cathode Design for Proton Exchange Membrane Fuel Cells in Automotive Applications. *Automot. Innov.* **2021**, *4*, 144–164.
- (3) Chowdhury, A.; Bird, A.; Liu, J.; Zenyuk, I. V.; Kusoglu, A.; Radke, C. J.; Weber, A. Z. Linking Perfluorosulfonic Acid Ionomer Chemistry and High-Current Density Performance in Fuel-Cell Electrodes. ACS Appl. Mater. Interfaces 2021, 13, 42579–42589.
- (4) Kusoglu, A.; Weber, A. Z. New Insights into Perfluorinated Sulfonic-Acid Ionomers. *Chem. Rev.* **2017**, *117*, 987–1104.
- (5) Cullen, D. A.; Neyerlin, K. C.; Ahluwalia, R. K.; Mukundan, R.; More, K. L.; Borup, R. L.; Weber, A. Z.; Myers, D. J.; Kusoglu, A. New Roads and Challenges for Fuel Cells in Heavy-Duty Transportation. *Nat. Energy* **2021**, *6*, 462–474.
- (6) Paul, D. K.; Fraser, A.; Karan, K. Towards the Understanding of Proton Conduction Mechanism in PEMFC Catalyst Layer: Conductivity of Adsorbed Nafion Films. *Electrochem. Commun.* **2011**, 13, 774–777.
- (7) Dishari, S. K.; Hickner, M. A. Confinement and Proton Transfer in Nafion Thin Films. *Macromolecules* **2013**, *46*, 413–421.
- (8) Farzin, S.; Sarella, A.; Yandrasits, M. A.; Dishari, S. K. Fluorocarbon-Based Ionomers with Single Acid and Multiacid Side Chains at Nanothin Interfaces. *J. Phys. Chem. C* **2019**, *123*, 30871–30884.
- (9) Farzin, S.; Zamani, E.; Dishari, S. K. Unraveling Depth-Specific Ionic Conduction and Stiffness Behavior across Ionomer Thin Films and Bulk Membranes. *ACS Macro Lett.* **2021**, *10*, 791–798.
- (10) Chatterjee, S.; Obewhere, O. A.; Zamani, E.; Keloth, R.; Farzin, S.; Morton, M. D.; Sarella, A.; Dishari, S. K. Advancing Ionomer Design to Boost Interfacial and Thin-Film Proton Conductivity via a Styrene-Calix[4]Arene-Based Ionomers. *Cell Rep. Phys. Sci.* **2023**, *4*, 101282.
- (11) Hwang, M.; Nixon, K.; Sun, R.; Willis, C.; Elabd, Y. A. Sulfonated Pentablock Terpolymers as Membranes and Ionomers in Hydrogen Fuel Cells. *J. Membr. Sci.* **2021**, *633*, 119330.
- (12) Modestino, M. A.; Paul, D. K.; Dishari, S.; Petrina, S. A.; Allen, F. I.; Hickner, M. A.; Karan, K.; Segalman, R. A.; Weber, A. Z. Self-Assembly and Transport Limitations in Confined Nafion Films. *Macromolecules* **2013**, *46*, 867–873.
- (13) Sharon, D.; Bennington, P.; Liu, C.; Kambe, Y.; Dong, B. X.; Burnett, V. F.; Dolejsi, M.; Grocke, G.; Patel, S. N.; Nealey, P. F. Interrogation of Electrochemical Properties of Polymer Electrolyte Thin Films with Interdigitated Electrodes. *J. Electrochem. Soc.* 2018, 165, H1028–H1039.
- (14) Dishari, S. K.; Hickner, M. A. Antiplasticization and Water Uptake of Nafion® Thin Films. ACS Macro Lett. 2012, 1, 291–295.
- (15) Tesfaye, M.; MacDonald, A. N.; Dudenas, P. J.; Kusoglu, A.; Weber, A. Z. Exploring Substrate/Ionomer Interaction under Oxidizing and Reducing Environments. *Electrochem. Commun.* **2018**, 87, 86–90.
- (16) Ono, Y.; Nagao, Y. Interfacial Structure and Proton Conductivity of Nafion at the Pt-Deposited Surface. *Langmuir* **2016**, 32, 352–358.
- (17) Ohira, A.; Kuroda, S.; Mohamed, H. F. M.; Tavernier, B. Effect of Interface on Surface Morphology and Proton Conduction of Polymer Electrolyte Thin Films. *Phys. Chem. Chem. Phys.* **2013**, *15*, 11494–11500.

- (18) Kawamoto, T.; Aoki, M.; Kimura, T.; Chinapang, P.; Mizusawa, T.; Yamada, N. L.; Nemoto, F.; Watanabe, T.; Tanida, H.; Matsumoto, M.; Imai, H.; Miyake, J.; Miyatake, K.; Inukai, J. Sublayered Structures of Hydrated Nafion® Thin Film Formed by Casting on Pt Substrate Analyzed by X-Ray Absorption Spectroscopy under Ambient Conditions and Neutron Reflectometry at Temperature of 80 °C and Relative Humidity of 30–80%. *Electrochemistry* **2019**, *87*, 270–275.
- (19) Poojary, S.; Islam, M. N.; Shrivastava, U. N.; Roberts, E. P. L.; Karan, K. Transport and Electrochemical Interface Properties of Ionomers in Low-Pt Loading Catalyst Layers: Effect of Ionomer Equivalent Weight and Relative Humidity. *Molecules* **2020**, *25*, 3387.
- (20) Dishari, S. K.; Rumble, C. A.; Maroncelli, M.; Dura, J. A.; Hickner, M. A. Unraveling the Complex Hydration Behavior of Ionomers under Thin Film Confinement. *J. Phys. Chem. C* **2018**, *122*, 3471–3481.
- (21) Dura, J. A.; Murthi, V. S.; Hartman, M.; Satija, S. K.; Majkrzak, C. F. Multilamellar Interface Structures in Nafion. *Macromolecules* **2009**, 42, 4769–4774.
- (22) DeCaluwe, S. C.; Baker, A. M.; Bhargava, P.; Fischer, J. E.; Dura, J. A. Structure-Property Relationships at Nafion Thin-Film Interfaces: Thickness Effects on Hydration and Anisotropic Ion Transport. *Nano Energy* **2018**, *46*, 91–100.
- (23) Zimudzi, T. J.; Hickner, M. A. Signal Enhanced FTIR Analysis of Alignment in NAFION Thin Films at SiO2 and Au Interfaces. *ACS Macro Lett.* **2016**, *5*, 83–87.
- (24) Kushner, D. I.; Kusoglu, A.; Podraza, N. J.; Hickner, M. A. Substrate-Dependent Molecular and Nanostructural Orientation of Nafion Thin Films. *Adv. Funct. Mater.* **2019**, *29*, 1–10.
- (25) Kusoglu, A.; Dursch, T. J.; Weber, A. Z. Nanostructure/ Swelling Relationships of Bulk and Thin-Film PFSA Ionomers. *Adv. Funct. Mater.* **2016**, *26*, 4961–4975.
- (26) Xu, Z.; Yuan, S.; An, L.; Shen, S.; Xu, Q.; Yan, X.; Zhang, J. Effect of Substrate Surface Charges on Proton Conduction of Ultrathin Nafion Films. *ACS Appl. Mater. Interfaces* **2023**, *15*, 10735–10743.
- (27) Yagi, I.; Inokuma, K.; Kimijima, K.; Notsu, H. Molecular Structure of Buried Perfluorosulfonated Ionomer/Pt Interface Probed by Vibrational Sum Frequency Generation Spectroscopy. *J. Phys. Chem. C* **2014**, *118*, 26182–26190.
- (28) Mckechnie, D.; Cree, J.; Wadkin-snaith, D.; Johnston, K. Glass Transition Temperature of a Polymer Thin Film: Statistical and Fitting Uncertainties. *Polymer* **2020**, *195* (1–7), No. 122433.
- (29) DeCaluwe, S. C.; Kienzle, P. A.; Bhargava, P.; Baker, A. M.; Dura, J. A. Phase Segregation of Sulfonate Groups in Nafion Interface Lamellae, Quantified via Neutron Reflectometry Fitting Techniques for Multi-Layered Structures. *Soft Matter* **2014**, *10*, 5763–5776.
- (30) Kodama, K.; Motobayashi, K.; Shinohara, A.; Hasegawa, N.; Kudo, K.; Jinnouchi, R.; Osawa, M.; Morimoto, Y. Effect of the Side-Chain Structure of Perfluoro-Sulfonic Acid Ionomers on the Oxygen Reduction Reaction on the Surface of Pt. ACS Catal. 2018, 8, 694–700.
- (31) Farzin, S.; Johnson, T. J.; Chatterjee, S.; Zamani, E.; Dishari, S. K. Ionomers From Kraft Lignin for Renewable Energy Applications. *Front. Chem.* **2020**, *8*, 1–17.
- (32) Page, K. A.; Kusoglu, A.; Stafford, C. M.; Kim, S.; Kline, R. J.; Weber, A. Z. Confinement-Driven Increase in Ionomer Thin-Film Modulus. *Nano Lett.* **2014**, *14*, 2299–2304.
- (33) Nie, Y.; Zhou, Z.; Hao, T.; Ye, X.; Yang, W. The Distribution of Glass Transition Temperatures in Ultrathin Polymer Films Controlled by Segment Density or Interfacial Interaction. *Macromol. Theory Simul.* **2016**, 25, 187–195.
- (34) Glor, E. C.; Angrand, G. V.; Fakhraai, Z. Exploring the Broadening and the Existence of Two Glass Transitions Due to Competing Interfacial Effects in Thin, Supported Polymer Films. *J. Chem. Phys.* **2017**, *146*, 20330.
- (35) Rotella, C.; Napolitano, S.; De Cremer, L.; Koeckelberghs, G.; Wubbenhorst, M. Distribution of Segmental Mobility in Ultrathin Polymer Films. *Macromolecules* **2010**, *43*, 8686–8691.

- (36) Zhang, W.; Douglas, J. F.; Starr, F. W. Why We Need to Look beyond the Glass Transition Temperature to Characterize the Dynamics of Thin Supported Polymer Films. *Proc. Natl. Acad. Sci. U.S.A.* **2018**, *115*, 5641–5646.
- (37) Chatterjee, S.; Zamani, E.; Farzin, S.; Evazzade, I.; Obewhere, O. A.; Johnson, T. J.; Alexandrov, V.; Dishari, S. K. Molecular-Level Control Over Ionic Conduction and Ionic Current Direction by Designing Macrocycle-Based Ionomers. *JACS Au* **2022**, *2*, 1144–1159.
- (38) Coote, J. P.; Kinsey, T.; Street, D. P.; Kilbey, S. M.; Sangoro, J. R.; Stein, G. E. Surface-Induced Ordering Depresses Through-Film Ionic Conductivity in Lamellar Block Copolymer Electrolytes. *ACS Macro Lett.* **2020**, *9*, 565–570.
- (39) Dishari, S. K. Current Understanding of Proton Conduction in Confined Ionomeric Systems. *J. Postdoc. Res.* **2014**, *2*, 30–39.
- (40) Paul, D. K.; McCreery, R.; Karan, K. Proton Transport Property in Supported Nafion Nanothin Films by Electrochemical Impedance Spectroscopy. *J. Electrochem. Soc.* **2014**, *161*, F1395–F1402.
- (41) Coote, J. P.; Adotey, S. K. J.; Sangoro, J. R.; Stein, G. E. Interfacial Effects in Conductivity Measurements of Block Copolymer Electrolytes. *ACS Polym. Au* **2023**, *3*, 331–343.
- (42) Ogata, Y.; Abe, T.; Yonemori, S.; Yamada, N. L.; Kawaguchi, D.; Tanaka, K. Impact of the Solid Interface on Proton Conductivity in Nafion Thin Films. *Langmuir* **2018**, *34*, 15483–15489.
- (43) Pramounmat, N.; Loney, C. N.; Kim, C.; Wiles, L.; Ayers, K. E.; Kusoglu, A.; Renner, J. N. Controlling the Distribution of Perfluorinated Sulfonic Acid Ionomer with Elastin-like Polypeptide. ACS Appl. Mater. Interfaces 2019, 11, 43649–43658.
- (44) Suter, T. A. M.; Smith, K.; Hack, J.; Rasha, L.; Rana, Z.; Angel, G. M. A.; Shearing, P. R.; Miller, T. S.; Brett, D. J. L. Engineering Catalyst Layers for Next-Generation Polymer Electrolyte Fuel Cells: A Review of Design, Materials, and Methods. *Adv. Energy Mater.* 2021, 11, 1–82.
- (45) Ohma, A.; Fushinobu, K.; Okazaki, K. Influence of Nafion® Film on Oxygen Reduction Reaction and Hydrogen Peroxide Formation on Pt Electrode for Proton Exchange Membrane Fuel Cell. *Electrochim. Act.* **2010**, *55*, 8829–8838.
- (46) Tymoczko, J.; Calle-Vallejo, F.; Colic, V.; Koper, M. T. M.; Schuhmann, W.; Bandarenka, A. S. Oxygen Reduction at a Cu-Modified Pt(111) Model Electrocatalyst in Contact with Nafion Polymer. ACS Catal. **2014**, *4*, 3772–3778.
- (47) Ott, S.; Du, F.; Luna, M. L.; Dao, T. A.; Cuenya, B. R.; Orfanidi, A.; Strasser, P. Understanding the Performance Increase of Catalysts Supported on N-Functionalized Carbon in PEMFC Catalyst Layers. J. Electrochem. Soc. 2022, 169, 054520.
- (48) Fang, S.; Liu, G.; Li, M.; Zhang, H.; Yu, J.; Zhang, F.; Pan, M.; Tang, H. Tailoring Ionomer Chemistry for Improved Oxygen Transport in the Cathode Catalyst Layer of Proton Exchange Membrane Fuel Cells. ACS Appl. Energy Mater. 2023, 6, 3590–3598.
- (49) Modestino, M. A.; Kusoglu, A.; Hexemer, A.; Weber, A. Z.; Segalman, R. A. Controlling Nafion Structure and Properties via Wetting Interactions. *Macromolecules* **2012**, *45*, 4681–4688.
- (50) Doo, G.; Yuk, S.; Lee, J. H.; Choi, S.; Lee, D. H.; Lee, D. W.; Hyun, J.; Kwon, S. H.; Lee, S. G.; Kim, H. T. Nano-Scale Control of the Ionomer Distribution by Molecular Masking of the Pt Surface in PEMFCs. J. Mater. Chem. A 2020, 8, 13004–13013.
- (51) Li, Y.; Hart, J.; Profitt, L.; Intikhab, S.; Chatterjee, S.; Taheri, M.; Snyder, J. Sequential Capacitive Deposition of Ionic Liquids for Conformal Thin Film Coatings on Oxygen Reduction Reaction Electrocatalysts. *ACS Catal.* **2019**, *9*, 9311–9316.
- (52) Li, Y.; Intikhab, S.; Malkani, A.; Xu, B.; Snyder, J. Ionic Liquid Additives for the Mitigation of Nafion Specific Adsorption on Platinum. *ACS Catal.* **2020**, *10*, 7691–7698.
- (53) Avid, A.; Ochoa, J. L.; Huang, Y.; Liu, Y.; Atanassov, P.; Zenyuk, I. V. Revealing the Role of Ionic Liquids in Promoting Fuel Cell Catalysts Reactivity and Durability. *Nat. Commun.* **2022**, *13*, 1–13.

- (54) Fan, L.; Wang, Y.; Jiao, K. Enhancing Oxygen Transport in the Ionomer Film on Platinum Catalyst Using Ionic Liquid Additives. *Fundam. Res.* **2022**, *2*, 230–236.
- (55) Li, Y.; Van Cleve, T.; Sun, R.; Gawas, R.; Wang, G.; Tang, M.; Elabd, Y. A.; Snyder, J.; Neyerlin, K. C. Modifying the Electrocatalyst Ionomer Interface via Sulfonated Poly(Ionic Liquid) Block Copolymers to Enable High- Performance Polymer Electrolyte Fuel Cells. ACS Energy Lett. 2020, 5, 1726–1731.
- (56) Sun, R.; Agrawal, M.; Neyerlin, K. C.; Snyder, J. D.; Elabd, Y. A. Proton Conducting Sulfonated Poly(Ionic Liquid) Block Copolymers. *Macromolecules* **2022**, *55*, 6716–6729.
- (57) Su, Z.; Kole, S.; Harden, L. C.; Palakkal, V. M.; Kim, C.; Nair, G.; Arges, C. G.; Renner, J. N. Peptide-Modified Electrode Surfaces for Promoting Anion Exchange Ionomer Microphase Separation and Ionic Conductivity. *ACS Mater. Lett.* **2019**, *1*, 467–475.
- (58) Farzin, S.; Acurio Cerda, K.; Obewhere, O. A.; Dishari, S. K. Lignin-Based Materials for Energy Conversion and Storage Devices. In *Sustainability Engineering Challenges, Technologies, and Applications*; Tan, E. C. D., Ed.; Taylor & Francis Group, 2023; pp 1–60.
- (59) Zhang, F.; Srinivasan, M. P. Self-Assembled Molecular Films of Aminosilanes and Their Immobilization Capacities. *Langmuir* **2004**, 20, 2309–2314.
- (60) Chowdhury, S. A.; Lim, M. Characterization of the Surface Contribution to Fluorescence Correlation Spectroscopy Measurements. *Bull. Korean Chem. Soc.* **2011**, *32*, 583–589.
- (61) Sayıklı Simsek, C.; Nur Sonuc Karaboga, M.; Sezginturk, M. K. A New Immobilization Procedure for Development of an Electrochemical Immunosensor for Parathyroid Hormone Detection Based on Gold Electrodes Modified with 6-Mercaptohexanol and Silane. *Talanta* 2015, 144, 210–218.
- (62) Shrivastava, U. N.; Fritzsche, H.; Karan, K. Interfacial and Bulk Water in Ultrathin Films of Nafion, 3M PFSA, and 3M PFIA Ionomers on a Polycrystalline Platinum Surface. *Macromolecules* **2018**, *51*, 9839–9849.
- (63) Page, K. A.; Shin, J. W.; Eastman, S. A.; Rowe, B. W.; Kim, S.; Kusoglu, A.; Yager, K. G.; Stafford, G. R. In Situ Method for Measuring the Mechanical Properties of Nafion Thin Films during Hydration Cycles. ACS Appl. Mater. Interfaces 2015, 7, 17874—17883.
- (64) Kreuer, K. D.; Portale, G. A Critical Revision of the Nano-Morphology of Proton Conducting Ionomers and Polyelectrolytes for Fuel Cell Applications. *Adv. Funct. Mater.* **2013**, 23, 5390–5397.
- (65) Da Silva, J. S.; Carvalho, S. G. M.; Da Silva, R. P.; Tavares, A. C.; Schade, U.; Puskar, L.; Fonseca, F. C.; Matos, B. R. SAXS Signature of the Lamellar Ordering of Ionic Domains of Perfluorinated Sulfonic-Acid Ionomers by Electric and Magnetic Field-Assisted Casting. *Phys. Chem. Chem. Phys.* **2020**, 22, 13764—13779.
- (66) Siretanu, I.; Chapel, J. P.; Drummond, C. Substrate Remote Control of Polymer Film Surface Mobility. *Macromolecules* **2012**, *45*, 1001–1005.